The influence of oxygen partial pressure on the base oxide of chromia forming steels: The story prior to breakaway oxidation

Corrosion Science 213 (2023) 110959

Contents lists available at ScienceDirect

Corrosion Science

journal homepage: www.elsevier.com/locate/corsci

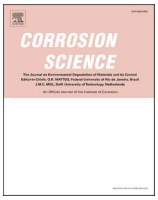

The influence of oxygen partial pressure on the base oxide of chromia forming steels: The story prior to breakaway oxidation

M. Sattari [b,*], H. Hooshyar [a], J. Liske [a], T. Jonsson [a]

[a] Department of Chemistry and Chemical Engineering, Chalmers University of Technology, SE-412 96 Göteborg, Sweden
[b] Department of Physics, Chalmers University of Technology, SE-412 96 Göteborg, Sweden

ARTICLE INFO

Keywords:
Stainless steels
High temperature corrosion
Water vapor
Oxygen activity
TEM

ABSTRACT

The influence of pO_2 on the base oxide formed on 304 L stainless steel has been investigated at 600 °C. The alloy was exposed in 5%O_2-95%N_2 and 10%H_2-20%H_2O-Ar atmospheres and the initial stages of oxidation were analysed by TEM and EDX. In both environments, the thin scale consists of a Cr-rich oxide overlaid by a FeCrMn oxide. However, the subscale formed in H_2-H_2O is richer in Cr compared to the 5%O_2-95%N_2 case (~90 cation% and ~70 cation% respectively). The findings are in good agreement with thermodynamic calculations and can explain breakaway oxidation of marginal chromia forming steels in H_2-H_2O.

1. Introduction

Chromia forming stainless steels such as 304 L are widely used in high temperature applications due to their excellent oxidation/corrosion resistance. The high oxidation resistance relies on the formation of a dense, adherent Cr-rich corundum type oxide scale acting as a barrier separating the alloy from the oxidizing/corrosive environment [1–3]. The performance of such a layer in dry oxygen/air environments has been shown to be satisfactory and protective, exhibiting slow growth rate [2,4]. However, the environment and the alloy microstructure may influence the necessary Cr content in the alloy for corrosion protection.

Water and/or hydrogen in the environment is well known to cause breakaway oxidation of stainless steels [5–11]. Various explanations have been suggested in order to explain oxidation in the presence of water and/or hydrogen; for example Cr evaporation [12,13], micro-crack formation [14], hydrogen ingress and faster oxygen diffusion as OH^- [15]. Ehlers et al. [16] proposed that breakaway oxidation is triggered by high $H_2O^{(g)}/O_2$ ratio and penetration of water vapor molecules through the scale; they suggested that $H_2O^{(g)}$ molecules are preferentially adsorbed on the surface, excluding oxygen, leading to a gas-permeable non-protective oxide scale. The experimental findings in Ehlers et al. [16] study were investigated in an atomistic molecular dynamic modelling by Chialvo et al. [17] in which they suggested that at the very early stages prior to the high temperature oxidation, H_2O is preferentially adsorbed and displaces oxygen at the metal-fluid interface.

At low pO_2 Cr evaporation is not valid and several mechanisms have been suggested to explain the effect of water and/or hydrogen in low oxygen partial pressure. Hänsel et al. [7] suggested a linear combination of Cr interstitials and Cr vacancies diffusion-induced mass transfer can explain the scale growth in low pO_2 water and/or hydrogen containing environments. Quadakkers et al. [4] proposed that the presence of H_2O and/or H_2 changes the mass transport processes not only within the oxide scale but also in the base alloy presumably by hydrogen ingress. As a consequence of hydrogen ingress, inward diffusion of oxygen and hence internal oxidation of Cr is promoted which leads to breakaway oxidation. The change in transport process of oxygen to predominantly inward diffusion at low pO_2 was also reported by Zurek et al. [18].

The aim of the present paper is to investigate the initial oxidation of the stainless steel 304 L in dry O_2 and in H_2-H_2O environment (low pO_2) prior to breakdown of the protective scale. The work involves a detailed microstructural investigation of the oxide scales formed after breakaway in different corrosive environments as well as thermodynamic equilibrium calculations.

2. Material and methods

In this work a 304 L stainless steel with the nominal composition given in Table 1 has been investigated. 15 × 15 × 2 mm metal coupons were cut and sanded down to P1000 SiC abrasive paper and thereafter polished with 6 μm, 3 μm, and finally 1 μm diamond suspension. Then, the coupons were thoroughly washed with water and ultrasonically

* Corresponding author.
E-mail address: sattari@chalmers.se (M. Sattari).

https://doi.org/10.1016/j.corsci.2023.110959
Received 12 September 2022; Received in revised form 28 December 2022; Accepted 31 December 2022
Available online 2 January 2023

Table 1
Nominal composition of the 304 L stainless steel (weight %).

	Fe	Cr	Ni	Mn	Si	Mo	N	C
304 L	Balance	18.18	8.1	1.53	0.31	0.53	0.07	0.022

cleaned in acetone and ethanol baths.

The high temperature oxidation exposures were conducted in a tube furnace at 600 °C with flowing gas, at a rate of 200 ml/min, parallel to the sample surface. Two exposure atmospheres were used in this study:

1. The low oxygen partial pressure environment with the gas mixture of 10% H2- 20% H2O- Ar corresponding to an oxygen partial pressure of approximately 10–24 bar (10–19 Pa). One sample was exposed in this atmosphere for 1 hr and a mass gain of 0.17 mg/cm2 was recorded.
2. The high oxygen partial pressure environment, 5% O2- 95% N2, at which another sample was exposed for 24 h with a measured mass gain of 0.02 mg/cm2.

Microstructural characterization of the thermally grown oxide scales on the coupons after exposures were carried out by scanning electron microscopy (SEM) plan view imaging as well as scanning transmission electron microscopy (STEM) coupled with energy dispersive X-ray spectroscopy (EDX). Electron transparent cross-sections of the samples were prepared by focus ion beam (FIB) milling and in-situ lift-out technique in an FEI Versa™ 3D DualBeam™ microscope. For this, the carefully chosen regions of interest were protected against ion beam damage by depositing two layers of Pt, using the microscope's gas injection system, before milling. An FEI Titan 80–300 microscope operating at 300 kV coupled with an INCA X-Sight Oxford Instrument detector were used for scanning transmission electron microscopy (STEM) and chemical analysis by Energy dispersive X-ray spectroscopy (EDX). FEI TEM Imaging & Analysis (TIA) software was used for data acquisition and post processing. The THERMO-CALC program [19,20] with the database TCFE7 was employed for equilibrium thermodynamic calculations.

3. Results

Fig. 1 shows a plan view SEM image of the sample acquired with through-the-lens secondary electron (SE) detector of the sample exposed to 5% O_2- 95% N_2 for 24 h. The sample surface is covered with a thin protective oxide. This is in line with the mass gain of 0.02 mg/cm^2 corresponding to a 110 nm calculated thickness assuming a dense eskolaite (Cr_2O_3) layer. However, some regions are covered by a thicker iron rich oxide (not shown).

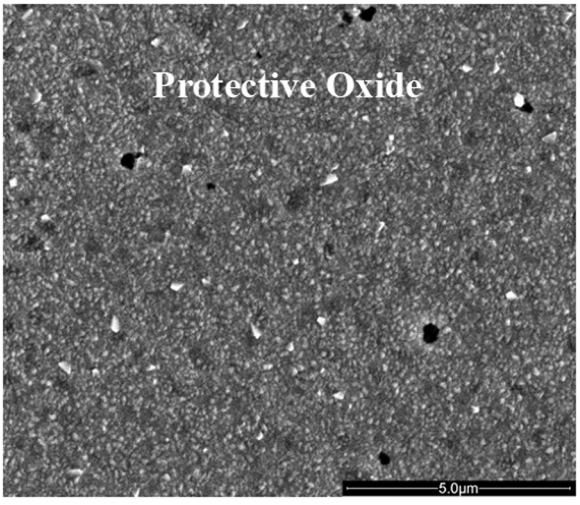

Fig. 1. Plan view secondary electron SEM image of the sample exposed to 5% O_2- 95% N_2 for 24 h.

Fig. 2 shows a STEM HAADF image of a cross-section of the sample shown in Fig. 1 (5% O_2- 95% N_2 for 24 h) taken from a region covered by a thin protective scale. The oxide thickness varies from about 20 nm to about 80 nm in the thicker regions/nodules. Voids were observed at the metal-oxide interface, particularly near the grain boundary in the metal.

Fig. 3 shows the results from an STEM/EDX line-scan along the line AC in Fig. 2. The scale is about 20 nm thick and has a Cr rich inner part (about 70 at% cations) and an Fe rich outer part. Below the oxide scale, an approximately 60 nm deep Cr-depleted region could be observed. The Cr content drops to about 4–7 at%.

Fig. 4 shows a scanning electron microscopy (SEM) plan view image of the H_2 +H_2O sample acquired by the through-the-lens secondary electron (SE) detector. The plan view image shows two types of morphology: 1- relatively thick oxide (indicative of breakaway oxidation in good correlation with the mass gain) covering almost the entire surface 2- Few isolated areas of about 20–30 µm in size covered by thin oxide. A cross-sectional sample for transmission electron microscopy (TEM) was extracted from the marked rectangular area. The morphology of the still thin protective scale is very similar to the morphology formed in dry oxygen. The morphology of the thicker part shows both grains and grain boundaries covered with oxide crystallites of about 1–2 µm in size; the grain boundaries seem to have a slightly thicker oxide probably due to faster diffusion rates.

Fig. 5 shows a scanning transmission electron microscopy (STEM) high angle annular dark field (HAADF) image of the cross-section extracted from the area indicated in Fig. 4. On the right the thin protective oxide scale can be seen and towards the left one can notice breakaway outward growing oxidation. The oxide thickness in the protective area varies between 50 and 100 nm.

Fig. 6 shows the results from a STEM/EDX line-scan along the line AC in Fig. 5. The scale is about 100 nm thick and has a Cr rich inner part (about 95 at% cations) and an Fe rich outer part. The alloy in a 100 nm region below the oxide scale is depleted in Cr. The content drops to about 5 at% in this region.

Fig. 7 shows the results from a STEM/EDX line-scan along the line DF in Fig. 5, i.e. a region covered by iron oxide. The scale is 140 nm thick and has a Cr rich inner part (about 95 at% cations) and an Fe rich outer part. The alloy in a 70 nm region below the oxide scale is excused in Cr. The content drops to about 1 at% in this region.

4. Discussion

Chromia forming stainless steels such as the investigated 304 L steel

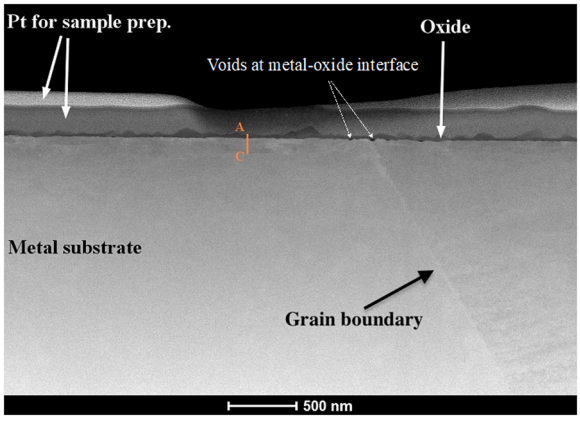

Fig. 2. High angle annular dark field (HAADF) scanning transmission electron microscope (STEM) image of the sample cross-section exposed to 5% O_2- 95% N_2 for 24 h (protective region).

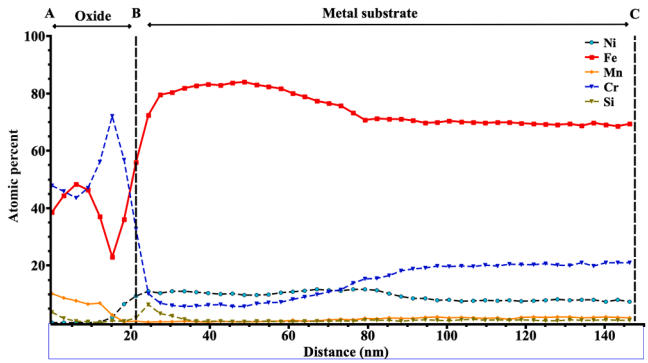

Fig. 3. Energy dispersive X-ray spectroscopy (EDX) line scan along the line AC in Fig. 2.

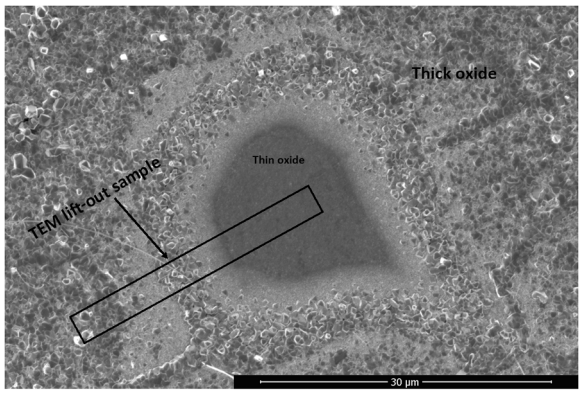

Fig. 4. Plan view SE image of the sample exposed to 10% H2- 20% H2O- Ar for 1 h; the marked area shows the region from which a lift-out cross section sample was prepared for TEM analysis.

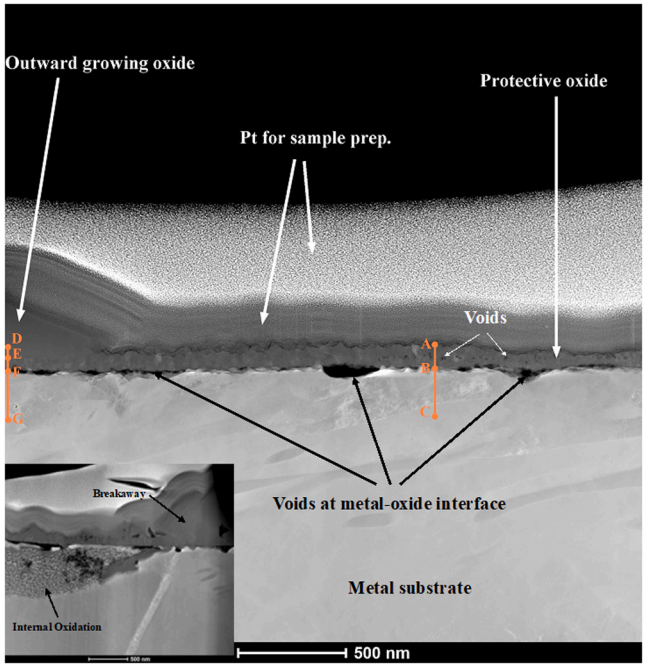

Fig. 5. High angle annular dark field (HAADF) scanning transmission electron microscope (STEM) image of the sample cross-section exposed to 10% H2- 20% H2O- Ar for 1 h. The inset shows the breakaway and internal oxidation region to the left.

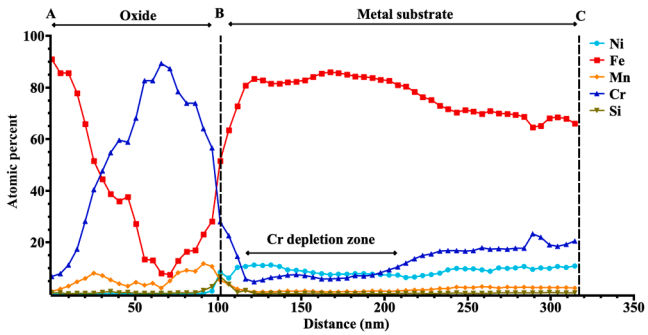

Fig. 6. Energy dispersive X-ray spectroscopy (EDX) line scan across the protective oxide (line AC in Fig. 5).

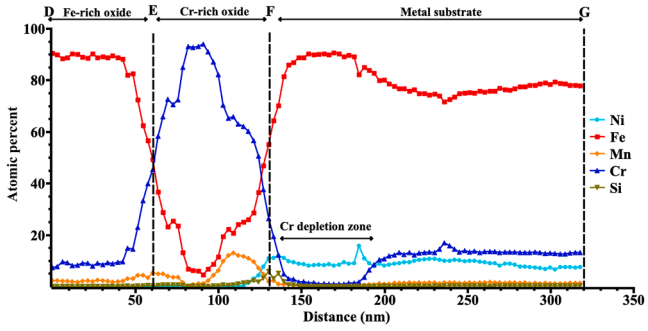

Fig. 7. Energy dispersive X-ray spectroscopy (EDX) line scan along the line DF in Fig. 5.

in the present study are well-known for their protective Cr-rich oxide scale when exposed to high temperatures in dry oxygen or air atmospheres [2,12,21,22]. There is a great amount of data in the literature on the oxidation of chromia forming stainless steels in dry oxygen atmospheres. Asteman et al. studied the oxidation behaviour of 304 L stainless steel both in dry and humid oxygen environments. Their gravimetry data as well as top view SEM images showed the presence of a protective scale after exposure to dry oxygen at 600 °C for up to 168 hr [12]. Tang et al. [22] investigated the microstructure and composition of the oxide scale formed on 304 L stainless[1] steel after 168 hr exposure in dry oxygen at 600 °C. They reported a Cr-rich $(Cr,Fe,Mn)_2O_3$ corundum type oxide layer with a Cr concentration profile which drops from about 70 cation% close to the metal-oxide interface to 25–34 cation % close to the gas-oxide interface. We also observed a protective oxide scale on 304 L stainless steel oxidized in 5% O_2- 95% N_2 at 600 °C for 24 h (Figs. 1 and 2). The oxide thickness was between 20 and 60 nm and consisted of two layers: 1- an iron-rich layer (about 48 cation % Fe) at the gas-oxide interface and underneath that a Cr-rich layer (about 70 cation % Cr) at the metal-oxide interface. This is in good agreement with the present results (see Figs. 1 and 2). In addition, The scale is very slow growing and has been shown to grow sub-parabolic/stepwise on both commercial alloys as 304 L and FeCr model alloys [23]. Thus, the initially formed Cr rich scale will remain protective in mild environments leaving a Cr depleted alloy with about 5 at% Cr below the scale.

In humid atmospheres and/or low oxygen partial pressures the oxide scale on chromia forming alloys is no longer protective and breakaway oxidation occurs [5–11]. In a related work, our detailed scanning transmission electron microscopy (STEM) analysis of the oxide scale after breakaway revealed the presence of a thin (40–50 nm) Cr-rich layer (about 55 cation % Cr and 45 cation % Fe) between the outward

[1] In the work by Tang et al. a 18–10 304 L stainless steel was studied while in the present study a 18–8 grade 304 L stainless steel is investigated

growing Fe-oxide and internal oxide region, i.e. at the original metal-oxide interface [24]. It is speculated that the Cr-rich layer is a remnant of the oxide initially formed at the original metal-oxide interface. The plan view SEM image in Fig. 4 shows that despite the very short exposure time almost the entire surface of the sample is covered by an iron oxide, i.e. breakaway oxidation. Only a few isolated islands such as the one in the middle of Fig. 4 remain protective. The HAADF cross-section image in Fig. 5 shows the transition from protective oxide on the right to breakaway area on the left. On the far left of the image characteristic features of breakaway oxidation in humid and/or low $p(O_2)$ environments, i.e. thick outward growing oxide can be seen; also further to the left internal oxidation was observed (inset in Fig. 5). These microstructural features following breakaway oxidation are discussed in detail in [25]. The focus of the present work is the protective oxide on the right hand side of the micrograph.

The oxide scale in the protective region and its corresponding EDX line scan (Fig. 5 and Fig. 6) reveal that the initial protective oxide consists of two layers: 1- An approximately 30 nm thick Fe-rich oxide (approximately 90 cation % Fe) on top, i.e. at the gas-oxide interface. 2- A Cr-rich oxide (about 90 cation % Cr) with a thickness of about 60 nm. The initial Cr-rich oxide formed in low $p(O_2)$ environment in the current work is different from the Cr-rich oxide scale formed in dry oxygen reported in the literature in a sense that it has a higher Cr content and is considerably thicker. The values for the latter case is around 70 cation % Cr after 24 hr oxidation, see Fig. 3. This is in good agreement with the Fe-Cr-O phase diagram $p(O_2)$ dependence at 600 °C shown in Fig. 8. According to this phase diagram, below a certain oxygen activity (around 10^{-14} bar (10^{-9} Pa)) the corundum stability phase boundary follows a steep slope towards 100% Cr (marked by the arrow in Fig. 8). This means that thermodynamically, only a very high Cr content corundum is stable at such low oxygen activities. Hence, The scale formed in high $p(O_2)$, i.e. $(Fe_xCr_{1-x})_2O_3$, remains stable with a Cr content of about 70%Cr while only very Cr-rich M_2O_3 (almost pure chromia) is stable below a $p(O_2)$ of about 10^{-14} bar (10^{-9} Pa).

It is well known that pure eskolaite (Cr_2O_3) grows considerably faster

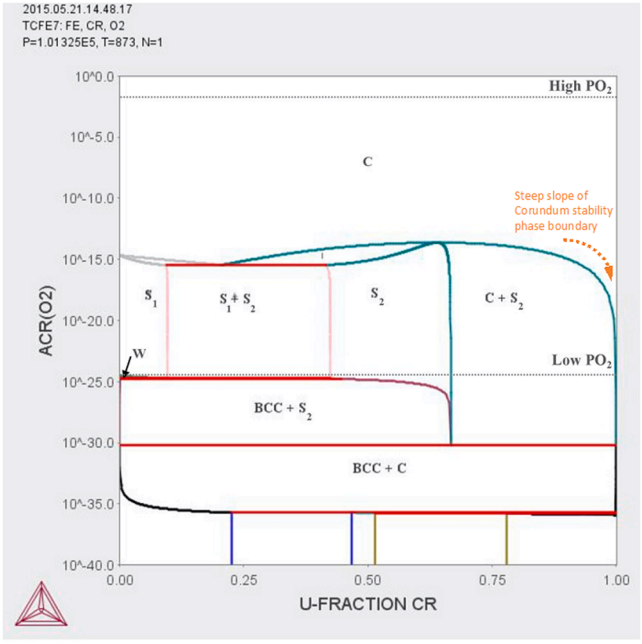

Fig. 8. Equilibrium phases in the Fe-Cr-O ternary system at 600 °C at different oxygen activities and Cr mole fractions. The diagram was generated employing the THERMO-CALC program with the TCFE7 database. C = corundum-type M_2O_3, $S_1 = Fe_{3-x}Cr_xO_4$, $S_2 = FeCr_{2-x}Fe_xO_4$, W= $Fe_{1-x}O$, BCC = ferritic metal. The dotted line indicates the oxygen activity in dry O_2 (high pO_2) and 10% H_2-20% H_2O- Ar (low pO_2).

than a Cr-rich M_2O_3 scale at 600 °C [23,26]. This is also supported by the present results. The Cr-rich scale formed in low $p(O_2)$ is about 50–100 nm after 1 h exposure while the scale formed at high $p(O_2)$ is about 20–80 nm after 24 h exposure. The different growth rates of the scales will generate a difference in Cr depletion beneath the scale assuming the diffusivities of Cr do not change due to the atmospheres, as proposed by Ani et al. [27]. A comparison of Cr-depletion depth in the metal substrate and Cr content in the depletion zone between the two above-mentioned environments is summarized in Table 2 (see below).

The scale formed in the low pO_2 environment contains a higher Cr content resulting in a faster growth rate followed by a Cr depletion/exhaustion in the alloy below the scale, see Table 2. It can be speculated that the formation and growth of the initial Cr-rich (90 cation % Cr) oxide scale depletes the substrate of Cr in the region close to metal-oxide interface. Hence, there remains mostly iron in the substrate near the metal-oxide interface which oxidizes and the resulting iron ions diffuse through the chromia layer and form the iron oxide layer at the gas-oxide interface. The Cr depletion depth and Cr content in depletion zone in the 1 hr sample in H_2 +H2O and 24 hr sample in 5% O_2- 95% N_2 (see Table 2) supports the mechanism.

The key point in the proposed breakaway mechanism in H_2 +H_2O environment is that the Cr content in the depletion zone, i.e. not in the protective oxide scale, must drop below a critical value in order for the breakaway to occur. This is supported by the EDX line-scan data in the breakaway region of the sample exposed to H_2 +H_2O for 1 hr (Fig. 7). Noticeable in this EDX line-scan is the drop of Cr content to about 1 at% in the depletion zone in metal substrate which should be compared to the corresponding value of 4.5–6 at% (Table 2) in the protective region (Fig. 3 and Fig. 4). The drop to a critical Cr content may thereby be linked to breakaway oxidation.

5. Conclusion

The oxide scales formed on 304 L stainless steel in H_2 +H2O and 5% O_2- 95% N_2 environments was investigated by means of scanning transmission electron microscopy (STEM) and energy dispersive X-ray spectroscopy (EDX). The comparison between the two oxide scales showed the followings:

1. The initial oxide formed in both environments consists of a Cr-rich layer at the metal-oxide interface and a Fe-rich layer above it at the oxide-gas interface.
2. The Cr-rich layer formed in H_2 +H2O has higher Cr content compared to the one formed in O_2-N_2 (about 90 cation % compared to about 71 cation % respectively)
3. The Cr content in the alloy substrate depletion zone beneath breakaway oxidation in H_2 +H2O drops down to 1 at%.

The above-mentioned observations are in good agreement with thermodynamic calculations of phase stability dependence on pO_2 within the Fe-Cr-O ternary system.

Declaration of Competing Interest

The authors declare that they have no known competing financial

Table 2
Cr depletion depth and Cr content in the depletion zone in metal substrate beneath the protective Cr-rich oxide formed in different environments.

	Cr depletion depth in metal substrate (nm)	Cr content in the depletion zone in substrate (at%)
H_2-H_2O – 1 h (protective area)	About 120	4.5 – 6
H_2-H_2O – 1 h (Breakaway area)	About 60	1
5% O_2 – 24 h	About 55	6

interests or personal relationships that could have appeared to influence the work reported in this paper.

Data Availability

Data will be made available on request.

Acknowledgements

This work was carried out within the High Temperature Corrosion Centre (HTC) at Chalmers University of Technology. The authors are grateful to Dr. Samuel Hallström at Thermo-Calc Software AB for discussing the Thermo-Calc calculations.

References

[1] P. Kofstad, High Temperature Corrosion, Elsevier Applied Science, 1998.
[2] D.J. Young, High Temperature Oxidation and Corrosion of Metals, First, 2008.
[3] H.E. Evans, A.T. Donaldson, Mechanisms of breakaway oxidation and application to a chromia-forming steel, Oxid. Met. 52 (1999).
[4] W.J. Quadakkers, J. Żurek, M. Hänsel, Effect of water vapor on high-temperature oxidation of FeCr alloys, Jom 61 (2009) 44–50, https://doi.org/10.1007/s11837-009-0102-y.
[5] S.R.J. Saunders, M. Monteiro, F. Rizzo, The oxidation behaviour of metals and alloys at high temperatures in atmospheres containing water vapour: a review, Prog. Mater. Sci. 53 (2008) 775–837, https://doi.org/10.1016/j.pmatsci.2007.11.001.
[6] E.D.L. Douglass, P. Kofstad, A. Rahmel, G.C. Wood, International workshop on high-temperature corrosion, Oxid. Met. 45 (1996).
[7] M. Hänsel, W.J. Quadakkers, D.J. Young, Role of water vapor in chromia-scale growth at low oxygen partial pressure, Oxid. Met. 59 (2003).
[8] E. Essuman, G.H. Meier, J. Żurek, M. Hänsel, W.J. Quadakkers, The effect of water vapor on selective oxidation of Fe–Cr alloys, Oxid. Met. 69 (2008) 143–162, https://doi.org/10.1007/s11085-007-9090-x.
[9] N.K. Othman, J. Zhang, D.J. Young, Water vapour effects on Fe-Cr alloy oxidation, Oxid. Met. 73 (2010) 337–352, https://doi.org/10.1007/s11085-009-9183-9.
[10] J. Chen, Z. Shen, J. Zhang, Effect of Water Vapor and Oxygen Partial Pressure on Oxidation of Fe and Fe–Cr Alloys, Springer, US, 2022. ⟨10.1007/s11085-022-10140-4⟩.
[11] T. Jonsson, B. Pujilaksono, H. Heidari, F. Liu, J.E. Svensson, M. Halvarsson, L. G. Johansson, Oxidation of Fe-10Cr in O2 and in O2+H2O environment at 600°C: a microstructural investigation, Corros. Sci. 75 (2013) 326–336, https://doi.org/10.1016/j.corsci.2013.06.016.
[12] H. Asteman, J. Svensson, L. Johansson, Evidence for chromium evaporation influencing the oxidation of 304L: the effect of temperature and flow rate, Oxid. Met. 57 (2002).
[13] N. Mu, K. Jung, N.M. Yanar, F.S. Pettit, G.R. Holcomb, B.H. Howard, G.H. Meier, The effects of water vapor and hydrogen on the high-temperature oxidation of alloys, Oxid. Met. 79 (2013) 461–472, https://doi.org/10.1007/s11085-012-9349-8.
[14] M. Schütze, M. Schorr, D.P. Renusch, A. Donchev, J.P.T. Vossen, The role of alloy composition, environment and stresses for the oxidation resistance of modern 9% Cr steels for fossil power stations, Mater. Res. 7 (2004) 111–123, https://doi.org/10.1590/S1516-14392004000100016.
[15] A. Galerie, Y. Wouters, M. Caillet, The kinetic behaviour of metals in water vapour at high temperatures: can general rules be proposed? Mater. Sci. Forum 369 (2001) 231–238.
[16] J. Ehlers, D.J. Young, E.J. Smaardijk, A.K. Tyagi, H.J. Penkalla, L. Singheiser, W. J. uadakkers, Enhanced oxidation of the 9%Cr steel P91 in water vapour containing environments, Corros. Sci. 48 (2006) 3428–3454, https://doi.org/10.1016/j.corsci.2006.02.002.
[17] A.A. Chialvo, M.P. Brady, J.R. Keiser, D.R. Cole, Modeling the effect of water vapor on the interfacial behavior of high-temperature air in contact with Fe20Cr surfaces, Scr. Mater. 64 (2011) 1027–1030, https://doi.org/10.1016/j.scriptamat.2011.02.013.
[18] J. Zurek, D.J. Young, E. Essuman, M. Hänsel, H.J. Penkalla, L. Niewolak, W. J. Quadakkers, Growth and adherence of chromia based surface scales on Ni-base alloys in high- and low-pO2 gases, Mater. Sci. Eng. A. 477 (2008) 259–270, https://doi.org/10.1016/j.msea.2007.05.035.
[19] J.O. Andersson, T. Helander, L. Hoglund, P. Shi, B. Sundman, Thermo-Calc & Dictra, computational tools for materials science, Calphad 26 (2002) 273–312. ⟨www.thermocalc.com⟩.
[20] B. Sundman, An assessment of the Fe-O system, J. Ph. Equilibria. 12 (1991) 127–140, https://doi.org/10.1007/BF02645709.
[21] M. Halvarsson, J.E. Tang, H. Asteman, J.-E. Svensson, L.-G. Johansson, Microstructural investigation of the breakdown of the protective oxide scale on a 304 steel in the presence of oxygen and water vapour at 600°C, Corros. Sci. 48 (2006) 2014–2035, https://doi.org/10.1016/j.corsci.2005.08.012.
[22] J.E. Tang, M. Halvarsson, H. Asteman, J. Svensson, The microstructure of the base oxide on 304L steel, 32 (2001) 799–805.
[23] B. Pujilaksono, T. Jonsson, H. Heidari, M. Halvarsson, J.E. Svensson, L. G. Johansson, Oxidation of binary FeCr alloys (Fe-2.25Cr, Fe-10Cr, Fe-18Cr and Fe-25Cr) in O 2 and in O 2 + H 2O environment at 600 °C, Oxid. Met. 75 (2011) 183–207, https://doi.org/10.1007/s11085-010-9229-z.
[24] H. Hooshyar, M. Sattari, T. Jonsson, J. Liske, J.-E. Svensson, L.-G. Johansson, A mechanistic study of high temperature oxidation of marginal chromia formers in presence of water vapor at low pO2 environment, Unpubl. Manuscr. (2016).
[25] T. Jonsson, S. Karlsson, H. Hooshyar, M. Sattari, J. Liske, J.-E. Svensson, L.-G. Johansson, Oxidation after breakdown of the chromium-rich scale on stainless steels at high temperature: internal oxidation, Oxid. Met. (2016), https://doi.org/10.1007/s11085-016-9610-7.
[26] B. Pujilaksono, T. Jonsson, M. Halvarsson, I. Panas, J.E. Svensson, L.G. Johansson, Paralinear oxidation of chromium in O 2 + H 2O environment at 600-700 °c, Oxid. Met. 70 (2008) 163–188, https://doi.org/10.1007/s11085-008-9114-1.
[27] M.H. Bin Ani, T. Kodama, M. Ueda, K. Kawamura, T. Maruyama, The effect of water vapor on high temperature oxidation of Fe-Cr alloys at 1073 K, Mater. Trans. 50 (2009) 2656–2663, https://doi.org/10.2320/matertrans.M2009212.